ARTICLE TEMPLATE

Temporal and spatial resolutions of optical time stretch imaging with dispersive grating pair

Lei Yang[a] and Qian Zhu[a] and Chao Wang[b] and Hui Chen[a] and Jincheng Li [a] and Hongbo Xie[a,*]

[a] School of Precision Instruments and Optoelectronics Engineering, Tianjin University Key Laboratory of Optoelectronics Information Technology, Ministry of Education, Tianjin, 300072, China

[b] School of Engineering and Digital Arts, University of Kent, Canterbury CT2 7NT, UK

ARTICLE HISTORY
Compiled October 2, 2019

ABSTRACT
Optical time stretch imaging (OTSI), providing the capability of capturing the dynamics of fast single-shot or random events, overcomes the fundamental trade-off between imaging speed and sensitivity in ultrafast imaging regions. Lying at the heart of the OTSI is dispersive Fourier transformation, being capable of using large chromatic dispersion to map the spectrum of a broadband ultrashort optical pulse into a stretched time-domain waveform. Dispersive grating pair (DGP) is an alternative solution to generate large chromatic dispersion for dispersive Fourier transformation at the wavebands, in which dispersion compensation fibers commonly suffer from high dispersion-to-loss ratio. Here we characterize the performances of DGP-based OTSI modality and analyze the crucial parameters that strongly impact on the temporal as well as spatial resolutions, and further discuss its merits and challenges. Our results demonstrate DGP-based OTSI, allowing creation of high resolution images, is an effective modality compared to fiber-based OTSI.

KEYWORDS
Ultrafast optical imaging; Time stretch imaging; Dispersive Fourier transformation; Dispersive grating pair; Temporal and spatial resolution

1. Introduction

Ultrafast imaging is becoming increasingly significant in observing transient phenomenon for diverse scientific and technological applications. Nowadays, pump-probe technique is one of the most prevalent strategies in fast-speed imaging regime which allows capturing repetitive dynamic events (*1*, *2*). However, this method is inapplicable for vast non-repeatable and random events because it is not operated in real-time (*3*). An alternative approach for measurement of the dynamic behaviour luminous events is using ultrafast framing streak camera, which has unique attributes of excellent time resolution and superior sensitivity (*4*, *5*). But high-cost of this instrument greatly limits its wide range of practical applications (*6*). To overcome the limitations in the existed methods, various fast optical imaging techniques have been rapidly developed in recent years.

*Email: hbxie@tju.edu.cn

Optical time stretch imaging (OTSI), also defined as serial time-encoded amplified microscopy (STEAM), is an impressive imaging approach that enables continuous capture of non-repetitive events at an unprecedented speed of tens of million frames per second (*7*, *8*). By adopting an all-optical imaging encoding concept, it captures the information of target with a single-pixel detector and offers great potentials to form images in various scenes that demand for both speed and throughput (*9*, *10*). The encoding procedure is normally divided into two steps: (i) wavelength-time mapping and (ii) space-wavelength mapping (*11*). The fist step, namely dispersive Fourier transformation, maps the broadband spectrum of an optical pulse into a temporal waveform using group velocity. In the second step, the spatial information of the specimen is encoded into the wavelength of the illuminating light. This novel imaging technique continuously captures a real-time frame of a rapid dynamic process because it slows the time scale before the image is detected by the digitizer (*12*).

In particular, temporal and spatial resolutions are two essential and equally important factors that are typically used to evaluate the performance of the OTSI system, which mainly rely on the procedure of time-stretch dispersive Fourier transform (TS-DFT) (*13*, *14*). The working principle of TS-DFT is employing group velocity dispersion (GVD) to map the frequency spectrum of a pulse to a time-stretched temporal waveform (*15*). Conventionally, the TS-DFT is carried out by utilization of dispersive elements to generate the quadratic phase modulation, and the image resolution is determined by the maximum amount of dispersion that is additionally introduced (*9*, *16*). Therefore, a dispersive optical element with large GVD and high dispersion-to-loss ratio is highly needed to achieve satisfactory imaging.

Dispersion compensating fibers (DCFs), the most used and commercially available technique for dispersion compensation, have successfully been employed for TS-DFTs (*7*, *15*). Nevertheless, DCF-based TS-DFTs were restricted at preferred transmission band (e.g. 1550 nm) where optical fiber has small loss (~ 0.5 dB/km) (*17*). For shorter near-infrared regimes (*18*) and 2.0 μm wavelength window (*19*), there remains huge challenge for implementing TS-DFT through DCFs, owing to the extremely high fiber transmission attenuation (~ 30 dB/km). TS-DFT could also be achieved by using a parallel pair of identical diffraction gratings, which offers distinct features of tunable temporal dispersion, low intrinsic loss as well as wavelength-insensitivity (*20*, *21*).

The purpose of this article is to give a quantitative analysis on the temporal and spatial resolutions for OTSI system with dispersive grating pair (DGP), which has not been discussed previously. The remainder of this article is organized as follows. Sec. 2 explains the theory and concept of dispersive Fourier transformation that maps the spectrum of an optical pulse into a temporal waveform using DGP. In Sec. 3, we present a detailed analysis on the temporal pulse stretching of the DGP system with second-order and third-order dispersion coefficients. The calculated and simulated results of temporal and spatial resolutions for OTSI system are demonstrated and reported in Sec. 4. Discussions on OTSI with higher-order dispersive Fourier transformation is presented in Sec. 5. Finally, we summarize and conclude our work in Sec. 6.

2. Time-stretch dispersive Fourier transform

The layout of DS-DFT with grating pair under consideration is schematically shown in Fig. 1. Considering the optical pulse propagates along with a homogeneous dispersive medium in z direction, electric field $U(z, T)$ satisfies the following equation (*22*)

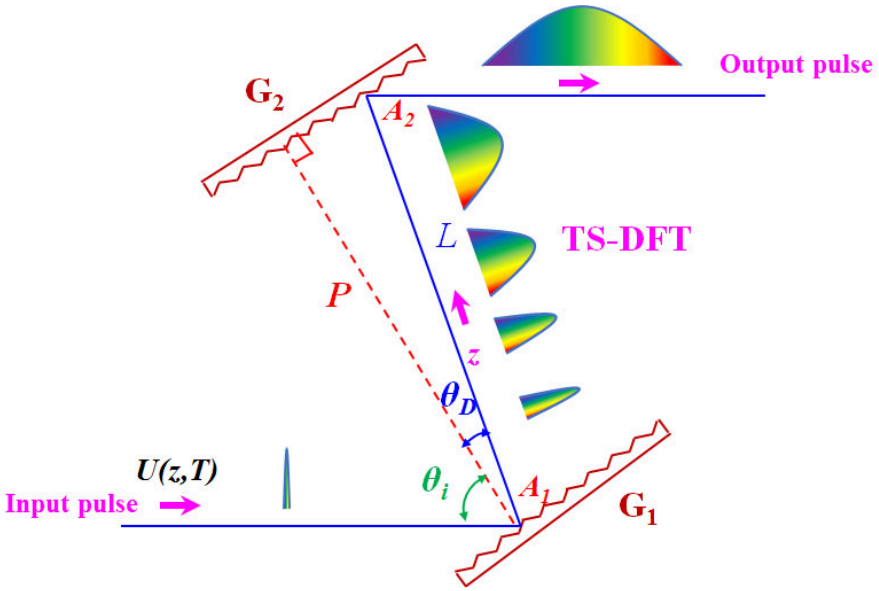

Figure 1. Principle of TS-DFT using a pair of parallel gratings. P, normal separation between two identical gratings; L, slant distance between two gratings; G, grating; θ_D, diffracted angle measured with respect to the grating normal.

$$\frac{\partial U(z,T)}{\partial z} = i\sum_{m=1}^{\infty}\frac{\beta_m}{m!}\frac{\partial^m U(z,T)}{\partial t^m} \tag{1}$$

z represents the propagation distance. T is measured in a frame of reference moving with the pulse at the group velocity, which is in the form

$$T = \beta_1 z - t \tag{2}$$

The wave number $\beta(\omega)$ can be expanded in a Taylor series with the carrier frequency ω_0

$$\beta_m = (\frac{d^m\beta}{d\omega^m})_{\omega=\omega_0} \qquad (m = 0, 1, 2, 3...) \tag{3}$$

Optical pulse propagation in Eq. (1) can be solved by using the Fourier-transform method

$$U(z,T) = \frac{1}{2\pi}\int_{-\infty}^{\infty}\tilde{U}(z,\omega)\exp(-i\omega T)d\omega \tag{4}$$

where

$$\tilde{U}(z,\omega-\omega_0) = \tilde{U}(0,\omega-\omega_0)\exp[i\sum_{m=2}^{\infty}\frac{\beta_m}{m!}(\omega-\omega_0)^m z] \tag{5}$$

Taking into account the GVD coefficients with up to the third-order, the optical pulse in time-domain after propagating distance z can be expressed as

$$U(z,T) = \frac{1}{2\pi}\int_{-\infty}^{\infty} \tilde{U}(0,\omega-\omega_0)\exp(\frac{i}{2}\beta_2(\omega-\omega_0)^2 z + \frac{i}{6}\beta_3(\omega-\omega_0)^3 z - i(\omega-\omega_0 t))d\omega \quad (6)$$

We apply the stationary phase approximation to solve the integral in Eq. (6). Assuming z is relatively large, even a small difference $(\omega-\omega_0)$ could produce rapid oscillations with the integral, which will cause cancellation (*23–25*). In Eq. (6), the phase term $i(\frac{\beta_2(\omega-\omega_0)}{2} + \frac{\beta_3(\omega-\omega_0)^3 z}{6} - (\omega-\omega_0)T)$ is stationary if it satisfies

$$\omega_0 = \sqrt{(\frac{\beta_2}{\beta_3})^2 + \frac{2T}{\beta_3 z}} - \frac{\beta_2}{\beta_3} \quad (7)$$

Moreover, when $\frac{T\beta_3}{z\beta_2^2} \ll 1$ is satisfied, Eq. (6) can be approximated by

$$\omega_0 \approx \frac{T}{\beta_2 z} \quad (8)$$

Spectral resolution $\Delta\omega$ is given by setting the phase in the integral (*23*)

$$\frac{\beta_2(\omega-\omega_0 \pm \frac{\Delta\omega}{2})}{2} + \frac{\beta_3(\omega-\omega_0 \pm \frac{\Delta\omega}{2})^3 z}{6} - (\omega-\omega_0 \pm \frac{\Delta\omega}{2})T = \frac{\pi}{2} \quad (9)$$

From which $\Delta\omega$ is found to be

$$\Delta\omega \simeq 2\sqrt{\frac{\pi}{\beta_2 z + \beta_3 z\omega_0}} \quad (10)$$

Ultimately, we find that

$$|U(z,T)| = \sqrt{\frac{2}{\pi[\beta_2 z + \beta_3 z\omega_0]}}|\tilde{U}(0,\omega_0)| \quad (11)$$

which implies the mapping of the spectrum of the input optical pulse into the time-domain waveform.

3. Optical pulse stretching with grating pair

DGP is valuable for optical time stretch because grating dispersion performs the desired temporal function for optical pulse with large spectral bandwidth, which is capable of leading wavelength-dependent optical delays to initial optical pulse (*26–29*). Specifically, the wavelength-dependent delay, also referring to frequency chirp, means temporal arrangement of the frequency components for the optical pulse. The temporal optical pulse is enormously stretched through DGP so that it is slow enough to be captured by a broadband detector and real-time oscilloscope.

Referring to the Fig. 1, the dispersive optical pulse stretcher is mainly comprised of two identical phase gratings with parallel configuration. When incoming on the first grating (G_1), the incident optical pulse is split into component wavelengths. The optical beams with different wavelengths propagate along the different directions between two gratings. After diffracted by the second grating (G_2), the optical beams with various propagating directions become parallel again, but they have traveled different distances. Therefore, the optical pulses with various wavelengths arrive different times in this DGP configuration.

When the optical pulse passes between grating pair, the frequency-dependent phase difference $\psi(\omega)$ between points A_1 and A_2 can be expressed as (*30*)

$$\psi(\omega) = -\frac{2\pi P(\omega)}{\lambda} = -\frac{\omega P(\omega)}{c} \tag{12}$$

The path length $P(\omega)$ is defined as

$$P(\omega) = Ln(\omega)\cos\theta_D(\omega) \tag{13}$$

where L and θ_D represent the slant distance between two gratings and diffracted angle, respectively. $n(\omega)$=1 when the light beam propagates in the air. In view of the relationship of $\omega = \frac{2\pi c}{\lambda}$, the first-order phase dispersion is found to be

$$\frac{\partial\psi(\omega)}{\partial\omega} = -\frac{P}{c} + \frac{\lambda}{c}\frac{\partial P}{\partial\lambda} \tag{14}$$

The second-order and third-order phase dispersions are given by

$$\frac{\partial^2\psi(\omega)}{\partial\omega^2} = -\frac{\lambda^3}{2\pi c^2}\frac{\partial^2 P}{\partial\lambda^2} \tag{15}$$

$$\frac{\partial^3\psi(\omega)}{\partial\omega^3} = \frac{\lambda^4}{4\pi^2 c^3}(3\frac{\partial^2 P}{\partial\lambda^2} + \lambda\frac{\partial^3 P}{\partial\lambda^3}) \tag{16}$$

According to the basic theory of phase grating, we derive

$$\sin\theta_D = \sin\theta_i + \frac{m\lambda}{d} \quad m = 0, \pm 1, \pm 2, ... \tag{17}$$

where θ_i, d and m stand for the incident angle, grating constant and diffraction order, respectively. The differentiating result of Eq. (17) is

$$\frac{d\theta_D}{d\lambda} = \frac{m}{d\cos\theta_D} \tag{18}$$

which yields

$$\frac{\partial^2 P}{\partial\lambda^2} = -\frac{m^2 L}{d^2\cos^3\theta_D} \tag{19}$$

$$\frac{\partial^3 P}{\partial\lambda^3} = -\frac{3m^3 L\sin\theta_D}{d^3\cos^5\theta_D} \tag{20}$$

The resulting dispersions in terms of phase are

$$\frac{\partial^2\psi(\omega)}{\partial\omega^2} = \frac{m^2\lambda^3 L}{2\pi c^2 d^2 cos^3\theta_D} \tag{21}$$

$$\frac{\partial^3\psi(\omega)}{\partial\omega^3} = -\frac{3m^2\lambda^4 L}{4\pi^2 c^3 d^2 cos^3\theta_D}[1+\frac{m\lambda}{d}\frac{sin\theta_D}{cos^2\theta_D}] \tag{22}$$

where $\psi(\omega)$ and β are commonly in the relationship

$$\psi(\omega) = -\beta L \tag{23}$$

For second-order and third-order dispersion coefficients, we have (*28*, *30*)

$$\beta_2 = -\frac{\partial^2\psi(\omega)}{\partial^2\omega}\cdot\frac{1}{L} = -\frac{m^2\lambda^3}{2\pi c^2 d^2 cos^3\theta_D} \tag{24}$$

$$\beta_3 = -\frac{\partial^3\psi(\omega)}{\partial\omega^3}\cdot\frac{1}{L} = \frac{3m^2\lambda^4}{4\pi^2 c^3 d^2 cos^3\theta_D}[1+\frac{m\lambda}{d}\frac{sin\theta_D}{cos^2\theta_D}] \tag{25}$$

The GVD in DGP is conveniently depicted in terms of the dispersion parameter D, which is

$$D = \int(\frac{4\pi c}{\lambda^3}\beta_2 + \frac{4\pi^2 c^2}{\lambda^4}\beta_3)d\lambda \tag{26}$$

Substituting the Eqs. (24) and (25) into Eq. (26), one finds that

$$D = \frac{m^2\lambda}{cd^2\cos^3\theta_D} + \frac{3m^3\sin\theta_D\lambda^2}{2cd^3\cos^5\theta_D} \tag{27}$$

After traveling through the DGP, the time-wavelength transformation is manipulated by the GVD. The group delay is given by

$$\tau(\lambda) = \int DLd\lambda = (\frac{m^2\lambda^2}{cd^2\cos^3\theta_D} + \frac{m^3\sin\theta_D\lambda^3}{2cd^3\cos^5\theta_D})L \tag{28}$$

where $\Delta\lambda$ is the bandwidth of the laser beam. Therefore, the time duration into which the laser spectrum is mapped can be calculated as

$$\Delta\tau = |D|L\Delta\lambda \tag{29}$$

In order to avoid the overlaps between consecutive pulses that are stretched in time-domain, the temporal duration $\Delta\tau$ is limited by the repetition rate R of laser ($\Delta\tau < R^{-1}$). Moreover, stretched duration $\Delta\tau$ is also requested to meet the response time of broadband photodiode.

On the basis of Eqs. (24) and (25), we first evaluate the second-order dispersion coefficient β_2 and third-order dispersion coefficient β_3 that vary with different experimental parameters, as shown in Fig. 2. More specifically, Fig. 2(a) exhibits the absolute value of β_2 rapidly decreases along with a greater diffraction constant while the β_3 also cuts down in the same case. Meanwhile, β_2 and β_3 have the completely opposite changing trends under different diffracted angles (see Fig. 2(b)). On account

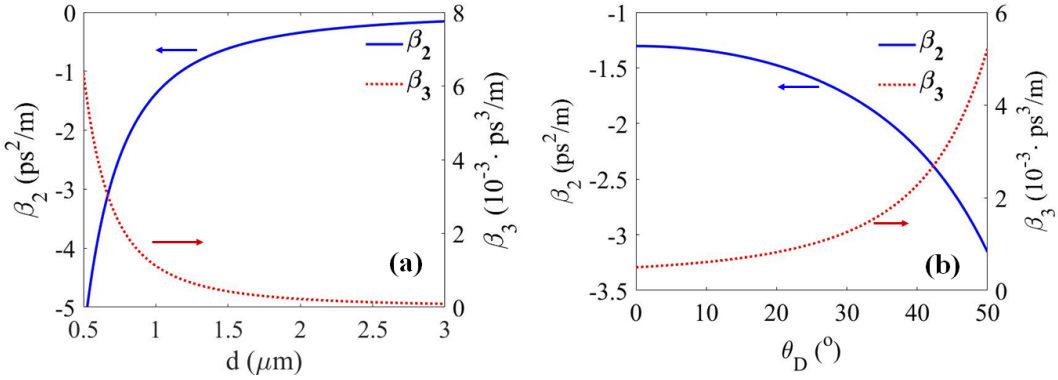

Figure 2. Second-order and third-order dispersion coefficients of DGP. (a) Varying with grating constant d. $\lambda = 800$ nm, $\theta_D = 22.5^0$ and $m = 1$. (b) Varying with diffracted angle θ_D. $\lambda = 800$ nm, $d = 1/1200$ mm and $m = 1$.

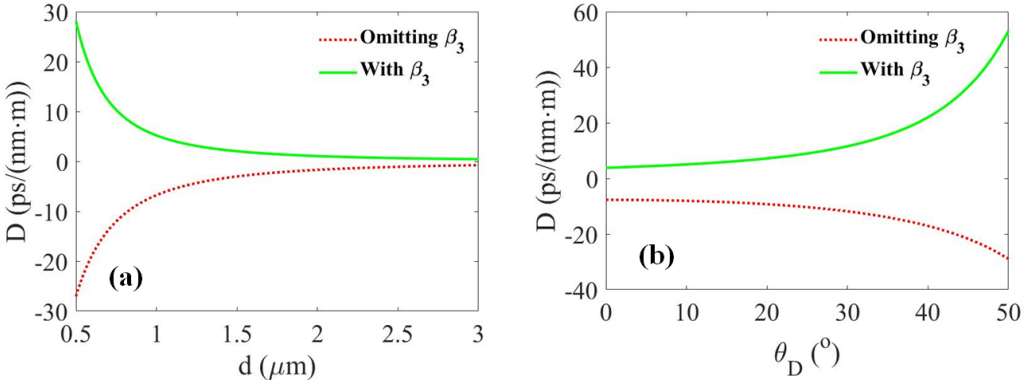

Figure 3. Dispersion parameter with and without third-order dispersion β_3. (a) Varying with diffraction constant d. $\lambda = 800$ nm, $\theta_D = 36^0$ and $m = 1$. (b) Varying with diffracted angle θ_D. The green solid line and red dotted line represent the calculated dispersion parameter D with and without β_3. $\lambda = 800$ nm, $d = 1/1200$ mm and $m = 1$. The expression of D without β_3 is $-\frac{2m^2\lambda}{cd^2\cos^3\theta_D}$.

of the expression of dispersion parameter D (Eq. (27)), we compare the value of D that is calculated with and without β_3, respectively, which is shown in Fig. 3. Simulation results further verify β_3 is a remarkably significant factor that is able to determine the value of D. Under the effect of β_3, the calculated dispersion parameter D always has the opposite value compared to the case if β_3 is omitted in calculation. Moreover, the results of stretched optical pulse with Eq. (29) are depicted in Fig.4, which indicate big diffracted angle and high-density grating are beneficial to acquire desired pulse with wide duration.

4. Temporal and spatial resolutions of OTSI

A typical setup of OTSI is composed of a frequency-to-time mapping module, a time-to-space mapping module, an ultrafast photodiode and a real-time oscilloscope. In frequency-to-time mapping part, the optical pulse propagates and reflects M times in the optical cavity between two parallel gratings (G_1 and G_2). This optical cavity consists of a pair of sliver-coated high reflective mirrors (HRMs) with separation distance q, which aims at largely improving the optical light path for sufficient dispersion and

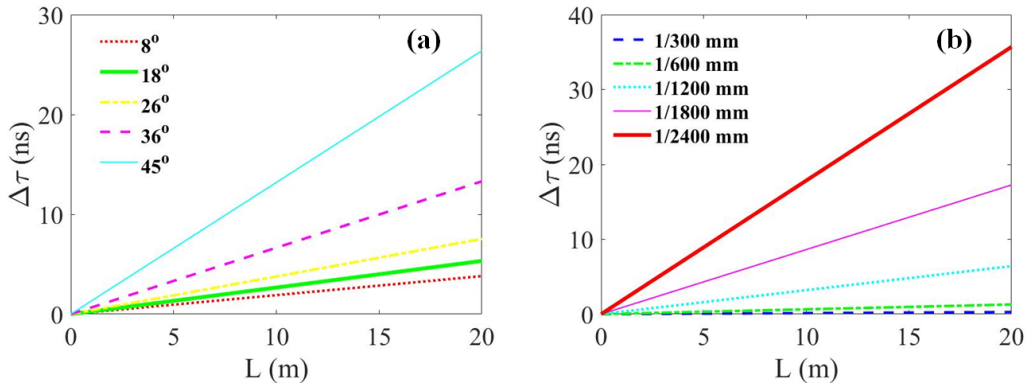

Figure 4. Width of optical pulse after propagating through DGP. (a) With different diffracted angles. The red dotted line, green thick line, yellow dotted-dashed line, purple dashed line and cyan thin line represent the diffracted angle θ_D of 8^o, 18^o, 26^o, 36^o and 45^o, respectively. $\lambda = 800$ nm, $\Delta\lambda = 40$ nm, $d = 1/1200$ mm and $m = 1$. (b) With different grating constants. The blue dashed line, green dotted-dashed line, cyan dotted line, purple thin line and red thick line represent the grating constant d of 1/300 mm, 1/600 mm, 1/1200 mm, 1/1800 mm and 1/2400 mm, respectively. $\lambda = 800$ nm, $\Delta\lambda = 40$ nm, $\theta_D = 22.5^0$ and $m = 1$.

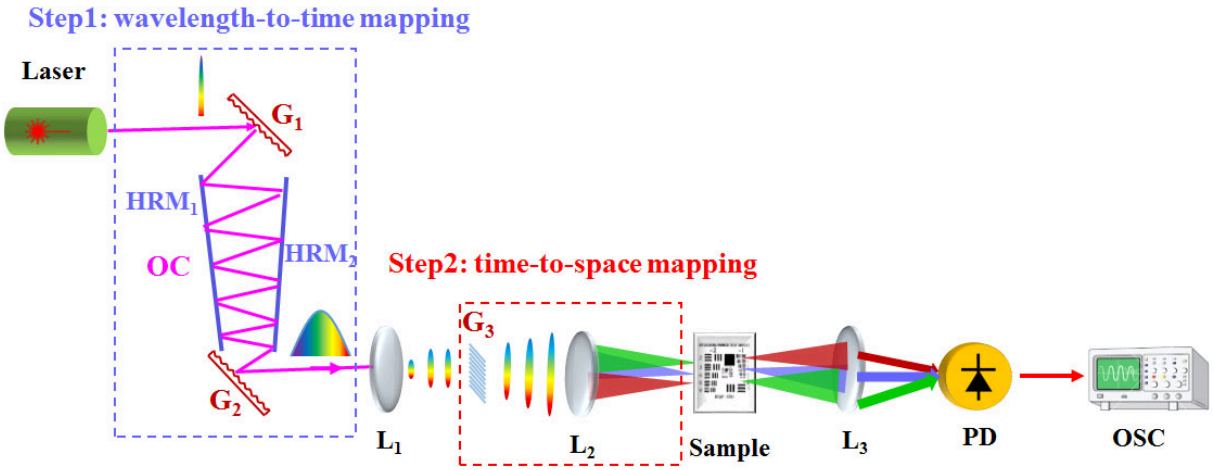

Figure 5. Conceptual configuration of OTSI system. G, grating; OC, optical cavity; HRM, high reflective mirror; L, lens; PD, photodiode; OSC, Oscilloscope. The total propagating distance for time stretched pulse in the cavity can be calculated as $L = M \cdot q$, where M is reflective times of optical pulse and q is the distance between two highly reflective mirrors. The information of employed laser includes $\Delta\lambda = 40$ nm, wavelength range of 780 nm to 820 nm and initial pulse duration of 0.023 ps.

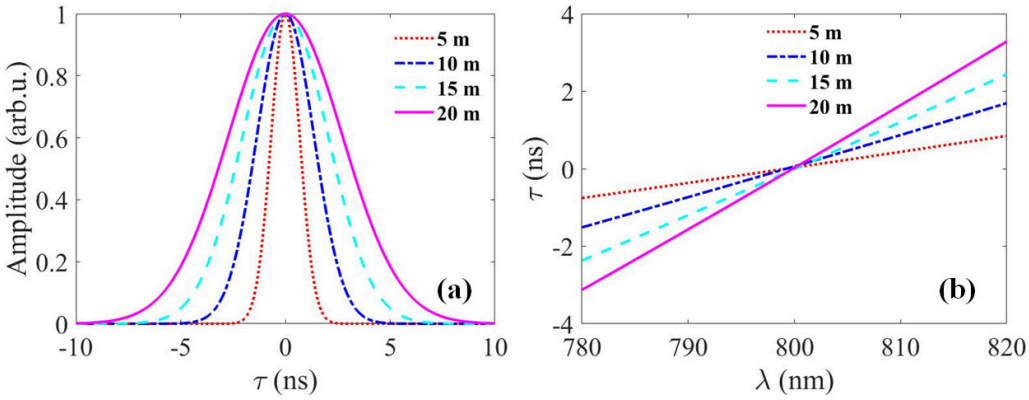

Figure 6. Physical description of wavelength-to-time mapping. (a) Optical pulse in time-domain when propagates in DGP. The temporal profile of optical pulse is plotted by $A = \exp(-\frac{\tau^2}{2(\Delta\tau/(2\sqrt{2In2}))^2})$. In addition, the original pulse width of input laser is 0.023 ps. (b) Time-to-wavelength mapping. The red dotted line, blue dotted-dashed line, cyan dashed line, purple solid line represent the propagation distance L of 5 m, 10 m, 15 m and 20 m, respectively. The plots are drawn by $\theta_D = 22.5^o$, $d = 1/1200$ mm, $m = 1$ and other essential parameters provided in the caption of Fig. 5.

compacting the practical configuration for time stretching in free-space (*31*). The used HRM could provide high reflectivity of 99.8% and wide bandwidth ranging from 0.4 to 10 μm. In contrast to the fiber-based devices, the proposed configuration however suffers from severe beam divergence in a long-distance propagation along two parallel gratings. Therefore, a tiny angle between two HRM surfaces ($\sim$ 0.2 to 3 mrad) is set to compress the intrinsic beam divergence induced by light propagation in the optical cavity. The time-to-space system operates in transmission mode, in which the spectrum of incident beam is spatially dispersed by the diffraction grating (G_3) and focused by the lens (L_2) onto the sample in the image plane. After the light passes through the sample and is focused by a convex lens (L_3), the temporal and spatial encoded beam is detected by a single pixel photodiode and captured by a real-time oscilloscope.

The straightforward way to understand the photonic time stretch procedure is through the wavelength-to-time mapping, which is conceptually depicted in Fig. 6. We assume the input optical pulse has a standard Gaussian shape, whose evolution process is depicted in Fig. 6(a) as the pulse travels in DGP with different distances. The relationship between group delay and wavelength in Eq. (28) results in a nonlinear time-to-wavelength mapping, as shown in Fig. 6(b). In addition, the properties of time-to-wavelength mapping also depend on distance between two gratings, diffracted angle as well as grating constant. The OTSI system, requiring high temporal and spatial resolutions, is close tied with this time-to-wavelength mapping procedure.

The temporal resolution regarding the spectral resolution $\Delta\omega$ is found to be (*13*)

$$\Delta T = \frac{dT}{d\omega}\Delta\omega = 2\sqrt{\pi[\beta_2 L + \beta_3 L\omega_0]} \tag{30}$$

where $L = M \cdot q$. In view of the relationship between angular frequency and wavelength, we can find

$$\Delta\omega = \frac{2\pi c}{\lambda^2}\Delta\lambda \tag{31}$$

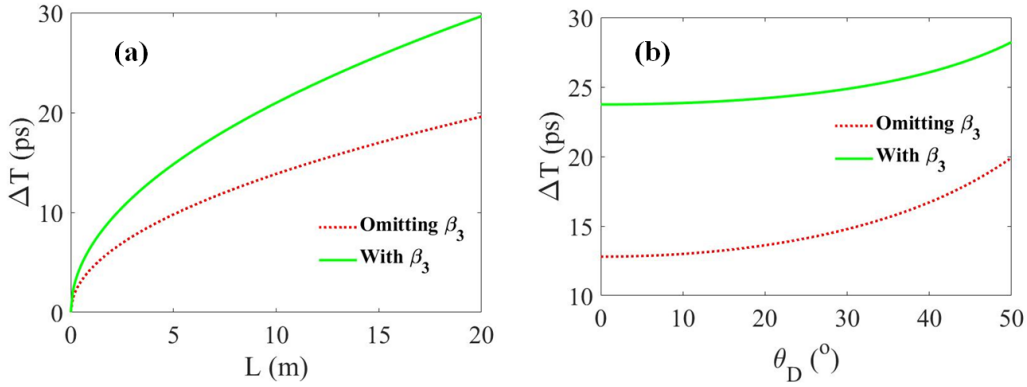

Figure 7. Comparison of temporal resolutions with and without third-order dispersion β_3. (a) Varying with slant distance L. $\theta_D = 22.5^o$, $d = 1/1200$ mm and $m = 1$. (b) Varying with diffracted angle θ_D. $L = 10$ m, $d = 1/1200$ mm and $m = 1$. The green solid line and red dotted line represent the calculated dispersion parameter D with and without β_3.

Consequently, the spectral resolution is written as

$$\Delta\lambda = \frac{\lambda^2}{c}\sqrt{\frac{1}{\pi(\beta_2 L + \beta_3 L\omega_0)}} \tag{32}$$

The spatial resolution can be found

$$\Delta X = \frac{\lambda^2 f}{c d_3 \cos(\theta_g)} \frac{1}{\sqrt{\pi[\beta_2 L + \beta_3 L\omega_0]}} \tag{33}$$

where d_3 and θ_g represent the grating constant and diffracted angle of G_3. In addition, f is the focal length of L_2.

Temporal resolution ΔT is obviously affected by the dispersion coefficient β_3 with longer propagation distance, which is shown in Fig. 7(a). Similarly, the curves of ΔT with and without β_3 appear tremendous difference when the diffracted angle θ_D increases (see Fig. 7(b)). As can be seen from Fig. 8(a) and (b), the plots ΔT varying with diffracted angles θ_D are quite different, and the simulated ΔT is also remarkable sensitive to the grating constant d. Accordingly, the attainable minimized value of time resolution ΔT, requires a high-density grating with a big diffracted angle. By contrast, the spatial resolution ΔX has an inversely proportional relationship with the temporal resolution ΔT, and its detailed descriptions related with experimental parameters are shown in Fig. 9 and 10, respectively. Therefore, it is not difficult to draw the conclusion that the performance of temporal and spatial resolutions are very often comprised in the implementation of a practical OTSI system.

The bandwidth of the detection system, including photodiode and oscilloscope, is also a limiting factor to determine the best achievable temporal and spatial resolutions. The inner relationships between DS-DFT through stationary phase approximation, spectral resolution of the spatial disperser and bandwidth of the detection system that all imposes on the system resolution have been comprehensively discussed in Ref. (*13*). Our work places great emphasis on investigating the principle of dispersive grating time stretch and its dramatic influence on the resolution of OTSI system.

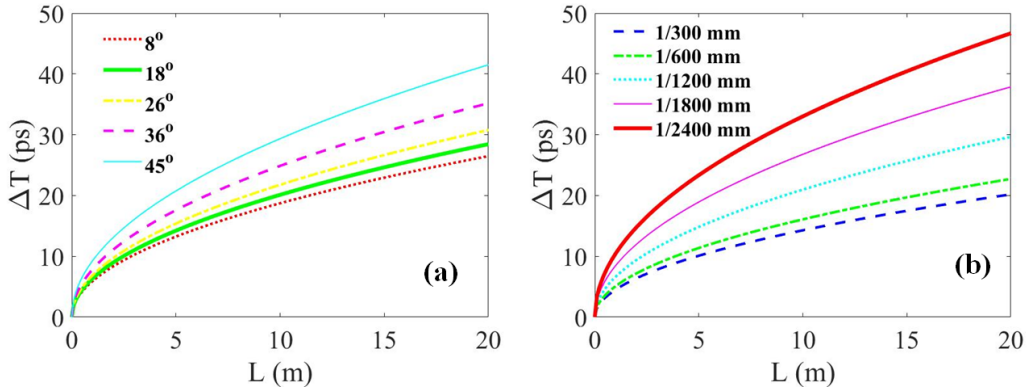

Figure 8. Temporal resolutions of OTSI system. (a) With different diffracted angles. The red dotted line, green thick line, yellow dotted-dashed line, purple dashed line and cyan thin line represent the diffracted angle θ_D of 8^o, 18^o, 26^o, 36^o and 45^o, respectively. $d = 1/1200$ mm and $m = 1$. (b) With different grating constants. The blue dashed line, green dotted-dashed line, cyan dotted line, purple thin line and red thick line represent the grating constant d of 1/300 mm, 1/600 mm, 1/1200 mm, 1/1800 mm and 1/2400 mm, respectively. $\theta_D = 22.5^o$ and $m = 1$. The plots are derived from Eq. (30).

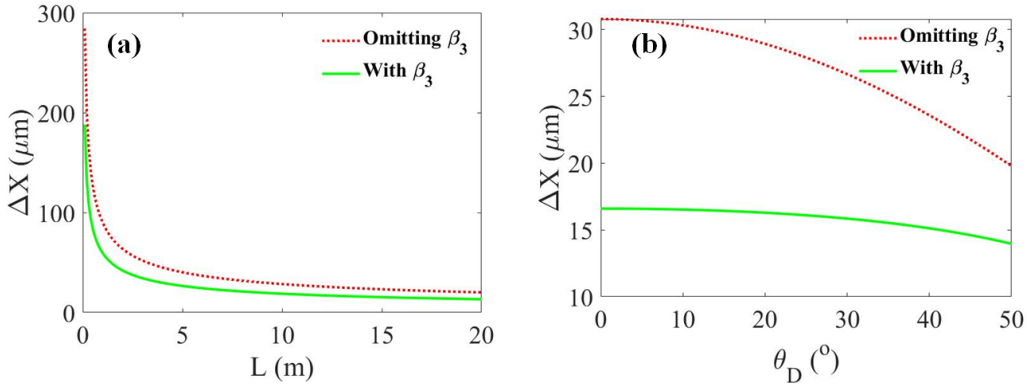

Figure 9. Comparison of spatial resolutions with and without third-order dispersion β_3. (a) Varying with slant distance L. $\theta_D = 22.5^o$, $d = 1/1200$ mm and $m = 1$. (b) Varying with diffracted angle θ_D. The green solid line and red dotted line represent the calculated dispersion parameter D with and without β_3. $L = 10$ m, $d = 1/1200$ mm and $m = 1$.

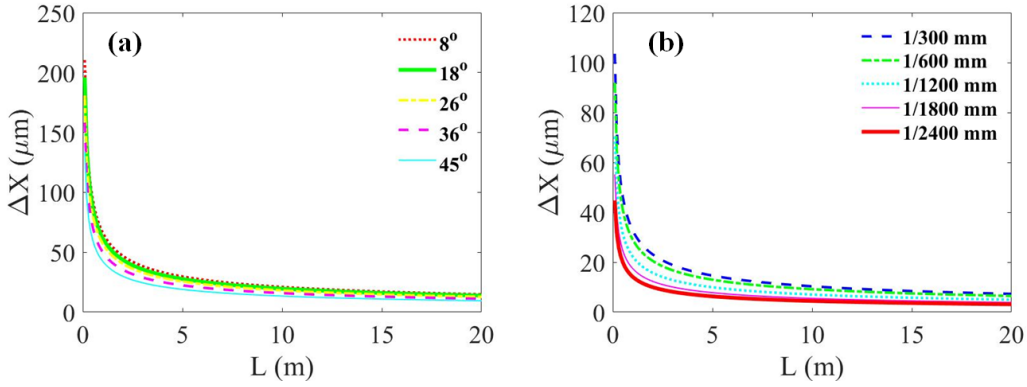

Figure 10. Spatial resolutions of OTSI system. (a) With different diffracted angles. The red dotted line, green thick line, yellow dotted-dashed line, purple dashed line and cyan thin line represent the diffracted angle θ_D of 8^o, 18^o, 26^o, 36^o and 45^o, respectively. $d = 1/1200$ mm and $m = 1$. (b) With different grating constants. The blue dashed line, green dotted-dashed line, cyan dotted line, purple thin line and red thick line represent the grating constant d of 1/300 mm, 1/600 mm, 1/1200 mm, 1/1800 mm and 1/2400 mm, respectively. $\theta_D = 22.5^o$ and $m = 1$. The plots are derived from Eq. (33).

5. OTSI system with higher-order dispersion coefficients

In this section, we now turn our attention to the higher-order dispersive effects of DGP. We add the higher-order dispersion coefficients in Eq. (1), the generalized spectral width is given by

$$\Delta\omega \simeq 2\sqrt{\frac{\pi}{\Sigma_{m=0}^{\infty}\frac{\beta_{m+2}}{m!}z\omega_0^m}} \tag{34}$$

Mapping the spectrum of the input pulse $|U(0,\omega)|$ into the time-domain waveform $|U(z,t)|$ with all GVD coefficients included is expressed as

$$|U(z,T)| = \sqrt{\frac{2}{\pi[\Sigma_{m=0}^{\infty}\frac{\beta_{m+2}}{m!}z\omega_0^m]}}|\tilde{U}(0,\omega_0)| \tag{35}$$

When the fourth-order term in expansion of Eq. (3) is not negligible, we firstly find the expression of fourth-order phase dispersion

$$\frac{\partial^4\psi(\omega)}{\partial\omega^4} = -\frac{\lambda^5}{2\pi^3c^4}(3\frac{\partial^2 P}{\partial\lambda^2} + \frac{7\lambda}{4}\frac{\partial^3 P}{\partial\lambda^3} + \frac{\lambda^2}{4}\frac{\partial^4 P}{\partial\lambda^4}) \tag{36}$$

where

$$\frac{\partial^4 P}{\partial\lambda^4} = -\frac{3m^4L}{d^4}\cdot\frac{1+4\sin^2\theta_D}{\cos^7\theta_D} \tag{37}$$

Therefore, Eq. (36) becomes

$$\frac{\partial^4\psi(\omega)}{\partial\omega^4} = \frac{3m^2\lambda^5L}{2\pi^3c^4d^2\cos^3\theta_D}(1 + \frac{7m\lambda\sin\theta_D}{4d\cos^2\theta_D} + \frac{m^2\lambda^2(1+4\sin^2\theta_D)}{4d^2\cos^4\theta_D}) \tag{38}$$

The four-order dispersion coefficient is in the form

$$\beta_4 = -\frac{3m^2\lambda^5}{2\pi^3c^4d^2\cos^3\theta_D}(1 + \frac{7m\lambda\sin\theta_D}{4d\cos^2\theta_D} + \frac{m^2\lambda^2(1+4\sin^2\theta_D)}{4d^2\cos^4\theta_D}) \tag{39}$$

In analogy with Eq. (30), the generalized temporal resolution with fourth-order dispersion, originated from spectral resolution, can be written as

$$\Delta T = \frac{dT}{dw}\Delta\omega = 2\sqrt{\pi(\beta_2 z + \beta_3 z\omega_0 + \frac{\beta_4}{2}z\omega_0^2)} \tag{40}$$

Finally, the spatial resolution including fourth-order dispersion is found to be

$$\Delta X = \frac{\lambda^2 f}{cd_3\cos(\theta_g)}\frac{1}{\sqrt{\pi[\beta_2 z + \beta_3 z\omega_0 + \frac{\beta_4}{2}z\omega_0^2]}} \tag{41}$$

6. Conclusion and outlook

Ultrafast optical imaging with the temporal resolution, being capable of achieving picosecond range, is a indispensable tool to study on rapid dynamic phenomena in biology, chemistry and physics. The photonic time-stretch technology has been found to be very valuable to address the intrinsic speed limitations on conventional imaging system, which uses TS-DFT procedure to slow down the temporal signal and in turn compress its bandwidth. However, the utilities of fiber-based TS-DFT imaging have been generally restrained at telecommunication band attributing to larger dispersion coming at the expense of higher loss in other spectral band, in particular the near infrared window for biological tissues.

DGP is a promising realization of group delay dispersions used to implement TS-DFT with a flexible operating spectrum, which converts the large angular dispersion into useful chromatic dispersion. In this article, we present the characterization for OTSI system building on DGP, a technique that leads to the ultrafast imaging in the extended optical band, and describe how these experimental parameters affect the properties of OTSI. The temporal and spatial resolutions, being relevant to second-order and third-order dispersion coefficients of DGP, are analyzed and discussed to estimate the performance of the proposed system. In summary, this work offers valuable insight to operation of OTSI system with DGP modality, which has unique features of high tunability, broadband and low substantial optical loss. Moving forward, high resolution DGP-based OTSI scheme, all-optical laser beam scanning system, also particularly enables ultrafast flow imaging and fluorescence imaging in modern biological fields.

Acknowledgement(s)

This work was supported in part by the National Natural Science Foundation of China (Grant No. 61875149), the Engineering and Physical Sciences Research Council (EPSRC) of UK (EP/S005625/1, EP/T51732X/1) and the Seed Foundation of Tianjin University, China (Grant No. 2018XZS-0011 and 2019XZS-0032).

References

(1) A. Barty et al. Ultrafast single-shot diffraction imaging of nanoscale dynamics. *Nature Photonics*, 2:415–419, 2008.

(2) M. Domke, S. Rapp, M. Schidt, and H. P. Huber. Ultrafast pump-probe microscopy with high temporal dynamic range. *Optics Express*, 20(9):10330–10338, 2012.

(3) S. Rapp, M. Kaiser, M. Schmidt, and H. P. Huber. Ultrafast pump-probe ellipsometry setup for the measurement of transient optical properties during laser ablation. *Optics Express*, 24(16):17572–17592, 2016.

(4) L. Gao, J. Yang, C. Li, and L. V. Wang. Singe-shot compressed ultrafast photography at one hundred billion frames per second. *Nature*, 516:74–77, 2014.

(5) L. Zhu, Y. Chen, J. Liang, Q. Xu, L. Gao, C. Ma, and L. V. Wang. Space- and intensity-constrained reconstruction for compressed ultrafast photography. *Optica*, 3(7):694–697, 2016.

(6) S. Patankar, E. T. Gumbrell, and T. S. Robinson et al. Absolute calibration of optical streak cameras on picosecond time scales using supercontinuum generation. *Applied Optics*, 56(24):6982–6987, 2017.

(7) K. Goda, K. K. Tsia, and B. Jalali. Serial time-encoded amplified imaging for real-time observation of fast dynamic phenomena. *Nature*, 458:1145–1149, 2009.
(8) G. Herink, B. Jalali, C. Ropers, and D. R. Solli. Resolving the build-up of femtosecond mode-locking with single-shot spectroscopy at 90 MHz frame rate. *Nature photonics*, 10:321–326, 2016.
(9) C. Wang. Dispersive fourier transformation for versatile microwave photonics applications. *Photonics*, 1:586–612, 2016.
(10) H. B. Xie, D. L. Ren, C. Wang, C. S. Wang, and L. Yang. Design of high-efficiency diffractive optical elements towards ultrafast mid-infrared time-stretched imaging and spectroscopy. *Journal of Modern Optics*, 65(3):255–261, 2017.
(11) K. Goda, A. Mahjoubfar, and C. Wang et al. Hybrid dispersion laser scanner. *Scientific Reports*, 2:445, 2012.
(12) Y. Han, O. Boyraz, and B. Jalali. Tera-sample per second real-time waveform digitizer. *Applied Physics Letters*, 87(24):241116, 2005.
(13) K. K. Tsia, K. Goda, D. Capewell, and B. Jalali. Performance of serial time-encoded amplified microscope. *Optics Express*, 18(10):10016–10028, 2010.
(14) G. Q. Wang, Z. J. Yan, L. Yang, L. Zhang, and C. Wang. Improved resolution optical time stretch imaging based on high efficiency in-fiber diffraction. *Scientific Reports*, 8:600, 2018.
(15) A. Mahjoubfar, D. V. Churkin, and S. Barland et al. Time stretch and its applications. *Nature Photonics*, 11:341–351, 2017.
(16) T. J. Parker. Dispersive fourier transform spectroscopy. *Contemporary Physics*, 31(5):335–353, 1990.
(17) L. Gruner-Nielsen, M. Wandel, and P. Kristensen et al. Dispersion-compensating fibers. *Journal of Lightwave Technology*, 23(11):3566–3579, 2005.
(18) C. Wang, K. Goda, M. Ibsen, and B. Jalali. Dispersive fourier transformation in the 800 nm spectral range. *2012 Conference on Lasers and Electro-Optics*, page ATu2G.2, 2012.
(19) S. Tian, L. Yang, and X. Wei et al. High-speed wavelength-swept source at 2.0 *mu*m and its application in imaging through a scattering medium. *Optics Letters*, 42(8):1540–1543, 2017.
(20) J. Wu, Y. Xu, and J. Xu et al. Ultrafast laser-scanning time-stretch imaging at visible wavelengths. *Light Science & Applications*, 6:e16196, 2017.
(21) S. Tian, X. Wei, and J. Wu et al. Flexible pulse-stretching for a swept source at 2.0 *mu*m using free-space angular-chirp-enhanced delay. *Optics Letters*, 43(1):102–105, 2018.
(22) S. A. Akhmanov and V. A. Vysloukh and A. S. Chirkin. *Optics of Femtosecond Laser Pulses*. American Institute of Physics, 1992.
(23) K. Goda, D. R. Solli, K. K. Tsia, and B. Jalai. Theory of amplified dispersive fourier transformation. *Physical Review A*, 80(4):043821, 2009.
(24) J. R. Klauder. Path integrals and stationary-phase approximations. *Physical Review D*, 19(8):2349–2356, 1979.
(25) D. Huber and E. J. Heller. Generalized gaussian wave packet dynamics, schrodinger equation, and stationary phase approximation. *The Journal of Chemical Physics*, 19(4):2003–2014, 1988.
(26) E. B. Treacy. Optical pulse compression with diffraction gratings. *IEEE Journal of Quantum Electronics*, QE-5(9):454–458, 1969.
(27) O. E. Martinez, J. P. Gordon, and R. L. Fork. Negative group-velocity dispersion using refraction. *Journal of the Optical Society of American A*, 1(10):1003–1006, 1984.
(28) M. Stern, J. P. Heritage, and E. W. Chase. Grating compensation of third-order fiber dispersion. *IEEE Journal of Quantum Electronics*, 28(12):2742–2748, 1992.
(29) M. Lai, S. T. Lai, and C. Swinger. Single-grating laser pulse stretcher and compressor. *Applied Optics*, 33(30):6985–6987, 1993.
(30) A. M. Weiner. *Ultrafast Optics*. Wiley, 2008.
(31) L. Yang, H. Chen, J. Ma, Q. Zhu, T. Yang, and H. B. Xie. Photonic time-stretch technology with prismatic pulse dispersion towards fast real-time measurements. *Photonics*,

6:9, 2019.